Improving color constancy in the presence of multiple illuminants using depth information

Marc Ebner and Johannes Hansen
Ernst-Moritz-Arndt-Universität Greifswald, Institut für Mathematik und Informatik,
Walther-Rathenau-Straße 47, 17487 Greifswald, Germany
marc.ebner@uni-greifswald.de

Keywords: Color Constancy, Space Average Color, Depth Map, Color, Kinect

Abstract: A human observer is able to judge the color of objects independent of the illuminant. In contrast, a digital sensor (or the retinal receptors for that matter) only measure reflected light which varies with the illuminant. The brain is somehow able to compute a color constant descriptor from the light falling onto the retina. We have improved a well known color constancy algorithm based on local space average color. This color constancy algorithm can be mapped to the different visual processing stages of the human brain. We have extended this algorithm by incorporating depth information. The idea is that wherever there are depth discontinuities there may also be a change of the illuminant in the image. Hence, depth discontinuities are used to separate different illuminants. This allows us to better estimate the local illumination and allows us to compute an improved color constant descriptor. We also compute local space average depth to decide locally whether to average data from retinal sensors uniformly or non-uniformly. We show how our algorithm works on real world scenes. Depth information is obtained from a standard Kinect sensor.

1 INTRODUCTION

Object color is an important cue in everyday life. We use it to recognize or distinguish different objects. However, color is a product of the brain (Zeki, 1993). The brain somehow computes a color constant descriptor from the data measured by the retinal receptors (Ebner, 2007a). The ability to compute a color constant descriptor is also very important for artificial vision systems. In particular, it is very important in the area of autonomous mobile robotics whenever robots have to work in several different environments.

In the human eye, the retinal receptors measure light reflected by objects. Unfortunately, reflected light varies with the spectral power distribution of the illuminant. Suppose a white wall is illuminated by an illuminant with a power distribution having a maximum in the red part of the spectrum. Hence the cones with a maximum absorption in the red part of the spectrum will respond more strongly than the cones with maximum absorption in the green and blue parts of the spectrum. Similarly, if we take a digital camera and take a digital photo of this scene, then the image will have a strong reddish color cast to it. The wall will appear red in the image. If the illuminant is known, we can compute a color corrected image of the scene. The scene will then look as if it had been illuminated by a uniform illuminant. Digital cameras assume that a single uniform illuminant (sunlight, cloudy sky, flash, neon light, etc.) is illuminating the scene. Hence, a digital camera corrects for a single illuminant. However, in practice this assumption (that a single illuminant is illuminating the scene) is not valid. We usually have multiple different illuminants such as sunlight falling through a window and artificial light turned on inside the building. Thus, we need to estimate the illuminant locally in order to correctly estimate object reflectance, i.e. the percentage of incident light which is reflected by an object. This estimate of object reflectance can then be used for object recognition as it is independent of the illuminant.

A number of different color constancy algorithms have been proposed (Agarwal et al., 2006; Ebner, 2007a). Most algorithms assume that a single uniform illuminant is illuminating the scene, e.g. the White Patch Retinex algorithm or the gray world assumption (Buchsbaum, 1980). Some algorithms assume that the illuminant is somehow constrained (Finlayson and Hordley, 2001). A color constancy algorithm based on the gray-edge hypothesis has been proposed by van de Weijer et al. (2007). Apart from the original

Retinex algorithm (Land and McCann, 1971), only a few work in the context of non-uniform illumination, e.g. Barnard et al.'s (1997) extension of the gamut constraint algorithm. In practice, one usually has to cope with a non-uniform illumination.

Most algorithms for color constancy cannot be readily mapped to the human vision system. Ebner (2007c; 2012) has proposed a model of human color perception which can be mapped to the human vision system. His method also works in the context of non-uniform illumination. In its original form, this algorithm only uses the output from the retinal receptors to arrive at a color constant descriptor. It does not use depth information. This algorithm has been extended by Ebner and Hansen (2013) to incorporate depth information. Here, we also compute local space average depth in order to decide locally whether to average data from retinal senors uniformly or non-uniformly. In addition, we better handle uncertainty in the position of the detected edges.

Depth information is readily available inside the human vision system. Gilchrist (1977) has put forward the coplanar ratio hypothesis. According to this hypothesis, lightness is determined primarily by ratios within perceived planes. Our research is in line with this hypothesis. How and if depth cues are actually used by the human visual system to compute a color constant descriptor is currently unknown. With this contribution we explore how depth information may be used to arrive at a color constant descriptor. For artificial vision systems, we can obtain depth information from a variety of methods (Horn, 1986; Jain et al., 1995). For our experiments, we have used the Kinect sensor to obtain a RGB image and the so called depth map which provides the distance to the corresponding object point for each pixel of the image.

In Section 2 we briefly explain Ebner's algorithm and how it can be mapped to the individual stages of the human vision system. In Section 3 we explain how depth information can be integrated into this algorithm. Section 4 describes how we have used the Kinect sensor to obtain a dense depth map. Section 5 describes the experiments that we have performed. Section 6 concludes this paper.

2 COLOR CONSTANCY BASED ON LOCAL SPACE AVERAGE COLOR

A color constant descriptor can be computed in various different ways. See Ebner (2007a) or Barnard et al. (2002) for an overview and evaluation of several different algorithms. A quite simple algorithm is the gray world assumption which has been put forward by Buchsbaum (1980). According to the gray world assumption, the world is gray on average. This assumption allows us to compute a color constant descriptor. Using this assumption, we can obtain an estimate of the illuminant by simply averaging all pixel values. Given this estimate, we can compute an output image that is independent of the illuminant. For the gray world assumption to work, it is necessary that quite a large number of different surface reflectances are contained in the scene being viewed.

Ebner (2009) has extended this algorithm to estimate the illuminant locally for each image pixel. He has also shown how this algorithm can be mapped to the human vision system (Ebner, 2007c, 2012). The algorithm runs on a grid of processing elements. It is assumed that we have one processing element per image pixel. For each pixel, we have three color bands in the red, green and blue parts of the spectrum. The processing elements are laterally connected to each other. Each processing element estimates the illuminant for the corresponding image pixel by computing local space average color. Let $\mathbf{a}(x,y) = [a_r(x,y), a_g(x,y), a_b(x,y)]$ be local space average color estimated by processing element at position (x,y). Let $\mathbf{c}(x,y) = [c_r(x,y), c_g(x,y), c_b(x,y)]$ be the measured color, i.e. the pixel color of the input image, at position (x,y). It is assumed that $\mathbf{c}(x,y)$ corresponds linearly to the irradiance falling onto the image sensor. Let $N(x,y)$ be the neighborhood defined for the processing element at position (x,y) and let p_c be a small positive value. The following two update equations are iterated until convergence:

$$a_i'(x,y) = \frac{1}{|N(x,y)|} \sum_{(x',y') \in N(x,y)} a_i(x',y') \qquad (1)$$

$$a_i(x,y) = (1-p_c) a_i'(x,y) + p_c c_i(x,y) \qquad (2)$$

with $i \in \{r,g,b\}$. The first equation takes local space average color from neighboring processing elements and averages it. The current element can also be included in this averaging process. The second equation adds a tiny amount of the measured color to the estimated average.

The parameter p_c determines the extent of the averaging. If p_c is rather small, then local space average color is computed over an extensive area. If p_c is comparatively large, then local space average color is computed over a very small area. The parameter p_c is usually set such that a sufficiently large number of image pixels are included in the average, e.g. 30% of all image pixels. Let $\bar{p}_c$ be the desired percentage of the image over which local space average color is computed and let s be the maximum of the width and

the height of the image in pixels, then p_c is given by $p_c = 1/(4 * \bar{p}_c^2 s^2)$.

Assuming narrow band sensors, then the measured irradiance is proportional to the reflectance $R_i(x,y)$ and irradiance $L_i(x,y)$ at the images object point for color band or wavelength i. In other words, we have $c_i(x,y) = L_i(x,y)R_i(x,y)$ assuming a scaling factor of 1. Using $L_i(x,y) \propto a_i(x,y)$ we can compute a color constant descriptor by dividing the measured color $c_i(x,y)$ by local space average color $a_i(x,y)$.

In Ebner's (2012) model, the retinal receptors measure the irradiance falling into the eye. The retinal receptors have a logarithmic response curve. The color space is rotated due to color opponent cells before reaching the visual cortex. Cells in V4 compute local space average color. This local space average color is subtracted from the data made available by cells in V1. Because of the logarithmic response, local space average color simply needs to be subtracted from the data from V1 in order to arrive at a color constant descriptor.

Within area V1, the visual stimulus is analyzed with respect to all kinds of different aspects (Livingstone and Hubel, 1984). Cells have been found whose optimal stimulus is an oriented line. Other cells' optimal stimulus is light of a particular wavelength. Cells usually respond more prominently to one eye or the other. These cells are grouped in columns which are called ocular dominance columns. It could be that visual information is also analyzed with respect to depth discontinuities in order to improve color perception. We will explore this possibility in the next section.

3 USING DEPTH INFORMATION TO IMPROVE COLOR CONSTANCY

In a natural scene, there are usually many different illuminants. Sun light may be falling through a window, a desk lamp may be turned on and at the same time neon light may illuminate the interior of the room. If we take an image of the room, the top of the desk may be illuminated by the light from the desk lamp while the area below the desk may be illuminated by ambient light which has been reflected multiple times by the objects contained in the room. If we look at the desk, we see a depth discontinuity at the edge of the desk which separates the top of the desk from the floor.

Figure 1(a) shows another example. The first room is illuminated by sunlight falling through a window while the corridor is illuminated by a blueish illuminant. For this image, the door frame provides a nice separation between the two illuminants. The depth discontinuity at the door frame has been highlighted manually.

We will now show how we can integrate such depth discontinuities into the algorithm to compute local space average color. It does not make sense to average local space average color across depth discontinuities because it is assumed that one illuminant illuminates the area on one side of the edge while another illuminant illuminates the area on the other side of the edge. Figure 1(b) shows an estimate of the two illuminants (computed by our algorithm). The two illuminants are clearly separated by the door frame. On the right hand side of the door we have a smooth illumination gradient. Figure 1(c) shows the output image which has been computed by dividing the measured color $\mathbf{c}(x,y)$ shown in Figure 1(a) by local space average color $\mathbf{a}(x,y)$ shown in Figure 1(b).

Of course it is also possible that the same illuminant illuminates both sides of an edge. However, this will do no harm. In order to take depth discontinuities into account, we only need to use a slightly modified neighborhood $N_d(x,y)$ which replaces the uniform neighborhood $N(x,y)$ in Equation (1). Let $d(x,y)$ be the depth map. The depth map specifies the distance from the camera to each object point. We only want to average across processing elements whose corresponding object points have approximately the same depth. Hence, we can define $N_d(x,y)$ as follows

$$\begin{aligned} N_d(x,y) = &\{(x',y') \in N(x,y) \\ &\text{with } |d(x,y) - d(x',y')| \leq \varepsilon_d(x,y)\} \end{aligned} \tag{3}$$

where ε_d defines the edge threshold assuming that the depth map has been scaled to the range $[0,1]$. We average across discontinuities smaller than $\varepsilon_d(x,y)$. Discontinuities larger than $\varepsilon_d(x,y)$ separate two processing elements in the averaging process.

The threshold ε_d can be set to a fixed value for the entire image. However, using a locally varying threshold may be more appropriate. Hence, we also compute local space average depth. Local space average depth $\tilde{d}$ is computed using the same method we have used to compute local space average color

$$\tilde{d}'(x,y) = \frac{1}{|N(x,y)|} \sum_{(x',y') \in N(x,y)} d_i(x',y') \tag{4}$$

$$\tilde{d}(x,y) = (1-p_d)\tilde{d}'(x,y) + p_d d(x,y) \tag{5}$$

where $d(x,y)$ is the depth value at position (x,y) and p_d is a small value which determines the extent of the averaging of the depth map. The parameter $\bar{p}_d$ is defined in exactly the same way as the parameter $\bar{p}_c$ above. Now that we have computed local space

(a) (b) (c)

Figure 1: (a) Sample image with two illuminants. The depth discontinuity separating the two illuminants has been manually highlighted in red. (b) Estimate of the illuminant. (c) Color constant descriptor.

average depth, we can make the threshold dependent on local depth. E.g. $\varepsilon_d(x,y) = 0.1\tilde{d}(x,y)$ means that we do not average across depth differences larger than 10% of the average depth in the region.

In practice, the alignment between the depth map and the color map may not be perfect. A non-perfect alignment between the depth map and the color image may result in artefacts at regions where the illuminant from another nearby region is used instead of the correct illuminant. That's why we first compute depth edges. A depth edge is located between two neighboring points (x,y) and (x',y') if we have $|d(x,y) - d(x',y')| > \varepsilon_d(x,y)$. We dilate the resulting binary edge image using a square structuring element of size 5×5. The size of the structuring element is set to the size of the uncertainty in the alignment between the depth map and the color image. The depth discontinuity is then assumed to be located inside this enlarged area at a location where we also have a color edge with a threshold of $\varepsilon_c = 0.1$. Because of this operation, depth discontinuities are now in perfect alignment with color edges in the image. If we have the unlikely case of a depth edge between two pixels but no color edge then our method will average across these pixels. In the human visual system, it is known that different aspects such as color, shape and motion are processed by different visual areas (Zeki, 1993; Zeki et al., 1991). It may be that these aspects are brought into alignment by a dynamic process similar to the one shown by Ramachandran (1993).

Figure 2 compares the two threshold methods for a real scene. Figure 2(a) shows the input image. Figure 2(b) shows local space average color computed with a fixed threshold for the entire image while Figure 2(c) shows local space average color computed with a spatially varying threshold as described above. The delineation of the border between the different illuminants is more accurate with a spatially varying threshold.

In the human vision system, binocular disparity can be used to estimate the distance of object points relative to the observer. For our experiments, we have used the Kinect to obtain a depth map for each input image.

4 OBTAINING A KINECT IMAGE ALIGNED DEPTH MAP

The Kinect sensor has been developed by Microsoft for the Xbox 360 video game console (Microsoft Corporation, 2011). It is a sensor which can be used for motion tracking and also sound position tracking. It consists of a horizontal bar with a RGB camera, a depth sensor, a multi-array microphone which rests on a motorized tilt unit as shown in Figure 3(a). Figure 3(b) shows the RGB image obtained with the Kinect sensor for a sample scene. The corresponding depth map is shown in Figure 3(c). A detailed description of the Kinect sensor is given by Kofler (2011). To date, it has been used in numerous different research projects. For instance, Newcombe et al. (2011), have shown how to perform dense surface mapping and tracking with the Kinect sensor. Gabel et al. (2012) have used it for full body gait analysis. A detailed evaluation of the Kinect sensor for computer vision applications is given by Andersen et al. (2012).

In order to use this depth map, we need to establish a correspondence between each image pixel of the input image and each pixel of the depth map. Color and depth sensors are a small distance apart from each other and they do not necessarily point into the same direction. The intrinsics and extrinsics of the sensors differ. The depth sensor covers a significantly smaller area than the color sensor. In addition, the depth sensor outputs data with a non-linear correspondence to distance.

We align the RGB input image and the depth map by performing a stereo calibration, i.e. computing intrinsic and extrinsic parameters of the two cam-

(a) (b) (c)

Figure 2: (a) Input image. (b) local space average color with a fixed threshold $\varepsilon_d(x,y) = \varepsilon_d$. (c) local space average color with a spatially varying threshold $\varepsilon_d(x,y) = 0.1\tilde{d}(x,y)$. In addition, depth discontinuities are aligned with color edges.

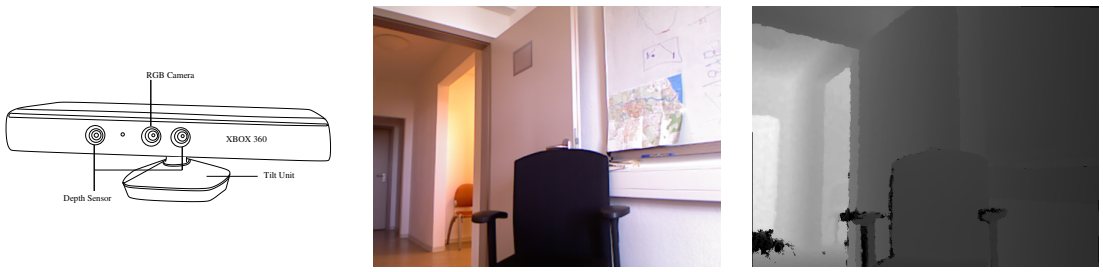

(a) (b) (c)

Figure 3: (a) Kinect sensor. (b) RGB image (c) Depth map.

eras and then transform the depth value to distance in meters. This approach is also described by Burrus (http://openkinect.org) and Kofler (2011). The Kinect sensor is not able to compute depth information for all pixels due to occlusion. Due to the arrangement of the infrared camera and the infrared laser which produces the laser grid for depth computation, the grid may not be visible for certain areas seen by the camera. This always happens to the left side of an edge. In order to accurately detect such edges, we need to compute a dense depth map from the Kinect output. We do this by iteratively filling in data from the left hand side. We call pixels for which the Kinect was able to estimate a depth value "a valid depth value" and we call all other pixels "invalid depth values". Before we apply our algorithm, we filter the depth map by removing isolated valid depth values which are surrounded by invalid depth values. These depth values are assumed to be incorrect. We then iterate n_f times over the image. Within each row with invalid pixels, we start from the left hand side and loop over all pixels with invalid depth values from left to right. Each pixel with an invalid depth value is updated by interpolating depth values from the top, upper left, left, lower left and the bottom side. The values from the top, left and bottom side use a weight of 1 while the diagonal pixels from the upper left and lower left use a weight of $1/\sqrt{2}$. We end up with a dense depth map which we can use for our algorithm.

5 EXPERIMENTS AND RESULTS

The algorithm is tested on a number of different images. Unfortunately, the Kinect only offers a relatively small field of view. The depth sensor provides data in the range from 0.8 to 3.5 meters with a depth resolution of 1cm at a distance of 2m (Andersen et al., 2012). This constrains the types of scenes that we can shoot. We have taken care to avoid shiny surfaces, such as mirrors, polished metals or brilliant varnishes in the scene. Such surfaces irritate the depth sensor. For dark scenes, noise can be removed by taking multiple images and then averaging the output.

The Kinect computes a depth map of size 640×480. The alignment algorithm corrects for the differences between the RGB image and the depth map. Since the RGB image and the depth map are not perfectly registered, we obtain a border around the image where depth is undefined. Hence, we crop the images to size 569×428 for further processing. The parameters were set to $\bar{p}_c = 0.25$, $\bar{p}_d = 0.1$, $\varepsilon_d(x,y) = 0.1\tilde{d}(x,y)$, $n_t = 15$ and $\varepsilon_c = 0.1$.

Figure 4 shows the results. For comparison Figure 5 through Figure 8 shows the estimate of the il-

luminant, i.e. local space average color for images 1 through 4, computed with three other color constancy algorithms: the gray world assumption (GW), standard local space average color (LSA) (Ebner, 2009), and computation of anisotropic local space average color along iso-illumination lines (Iso-LSA) (Ebner, 2007b). None of these methods use depth information. When we compare the results we see that depth information allows us to obtain a better estimate of the illuminant in the vicinity of depth edges.

6 CONCLUSIONS

We have shown how depth information can help in improving illumination estimates. A well known algorithm for color constancy based on local space average color has been updated to also include depth information. For our experiments, we have used the Kinect sensor to provide an RGB image with a corresponding depth map. Depth discontinuities in the depth map are assumed to separate different illuminants from each other. Our algorithm was tested on several different sample images. Comparison results with three other color constancy algorithms are also shown.

REFERENCES

Agarwal, V., Abidi, B. R., Koschan, A., and Abidi, M. A. (2006). An overview of color constancy algorithms. *Journal of Pattern Recognition Research*, 1(1):42–54.

Andersen, M. R., Jensen, T., Lisouski, P., Mortensen, A. K., Hansen, M. K., Gregersen, T., and Ahrendt, P. (2012). Kinect depth sensor evaluation for computer vision applications. Technical Report ECE-TR-6, Aarhus University, Denmark.

Barnard, K., Cardei, V., and Funt, B. (2002). A comparison of computational color constancy algorithms – part I and II. *IEEE Trans. on Image Processing*, 11(9):972–996.

Barnard, K., Finlayson, G., and Funt, B. (1997). Color constancy for scenes with varying illumination. *Computer Vision and Image Understanding*, 65(2):311–321.

Buchsbaum, G. (1980). A spatial processor model for object colour perception. *Journal of the Franklin Institute*, 310(1):337–350.

Ebner, M. (2007a). *Color Constancy*. John Wiley & Sons, England.

Ebner, M. (2007b). Estimating the color of the illuminant using anisotropic diffusion. In Kropatsch, W. G., Kampel, M., and Hanbury, A., eds., *Proc. of the 12th Int. Conf. on Computer Analysis of Images and Patterns, Vienna, Austria*, pp. 441–449, Berlin. Springer-Verlag.

Ebner, M. (2007c). How does the brain arrive at a color constant descriptor? In Mele, F., Ramella, G., Santillo, S., and Ventriglia, F., eds., *Proc. of the 2nd Int. Symp. on Brain, Vision and Artificial Intelligence, Naples, Italy*, pp. 84–93, Berlin. Springer.

Ebner, M. (2009). Color constancy based on local space average color. *Machine Vision and Applications Journal*, 20(5):283–301.

Ebner, M. (2012). A computational model for color perception. *Bio-Algorithms and Med-Systems*, 8(4):387–415.

Ebner, M. and Hansen, J. (2013). Depth map color constancy. Bio-Algorithms and Med-Systems (accepted).

Finlayson, G. and Hordley, S. (2001). Colour signal processing which removes illuminant colour temperature dependency. *UK Patent Application GB 2360660A*.

Gabel, M., Gilad-Bachrach, R., Renshaw, E., and Schuster, A. (2012). Full body gait analysis with Kinect. In *Proc. of the Annual Int. Conf. of the IEEE Engineering in Medicine and Biology Society, San Diego, CA*, pp. 1964–1967. IEEE.

Gilchrist, A. L. (1977). Perceived lightness depends on perceived spatial arrangement. *Science*, 195:185–187.

Horn, B. K. P. (1986). *Robot Vision*. The MIT Press, Cambridge, MA.

Jain, R., Kasturi, R., and Schunck, B. G. (1995). *Machine Vision*. McGraw-Hill, Inc., New York.

Kofler, M. (2011). Inbetriebahme und untersuchung des Kinect sensors. Master's thesis, FH Oberösterreich, Österreich.

Land, E. H. and McCann, J. J. (1971). Lightness and retinex theory. *Journal of the Optical Society of America*, 61(1):1–11.

Livingstone, M. S. and Hubel, D. H. (1984). Anatomy and physiology of a color system in the primate visual cortex. *The Journal of Neuroscience*, 4(1):309–356.

Microsoft Corporation (2011). Programming with the Kinect for Windows SDK.

Newcombe, R. A., Izadi, S., Hilliges, O., Molyneaux, D., Kim, D., Davison, A. J., Kohli, P., Shotton, J., Hodges, S., and Fitzgibbon, A. (2011). Kinectfusion: Real-time dense surface mapping and tracking. In *Proc. of the 10th IEEE Int. Symp. on Mixed and Augmented Reality*, pp. 127–136. IEEE.

Ramachandran, V. S. (1993). Filling in gaps in perception: Part II. Scotomas and phantom limbs. *Current Directions in Psychological Science*, 2(2):56–65.

van de Weijer, J., Gevers, T., and Gijsenij, A. (2007). Edge-based color constancy. *IEEE Trans. on Image Processing*, 16(9):2207–2214.

Zeki, S. (1993). *A Vision of the Brain*. Blackwell Science, Oxford.

Zeki, S., Watson, J. D. G., Lueck, C. J., Friston, K. J., Kennard, C., and Frackowiak, R. S. J. (1991). A direct demonstration of functional specialization in human visual cortex. *The Journal of Neuroscience*, 11(3):641–649.

Figure 4: Results of our algorithm for 4 sample images.

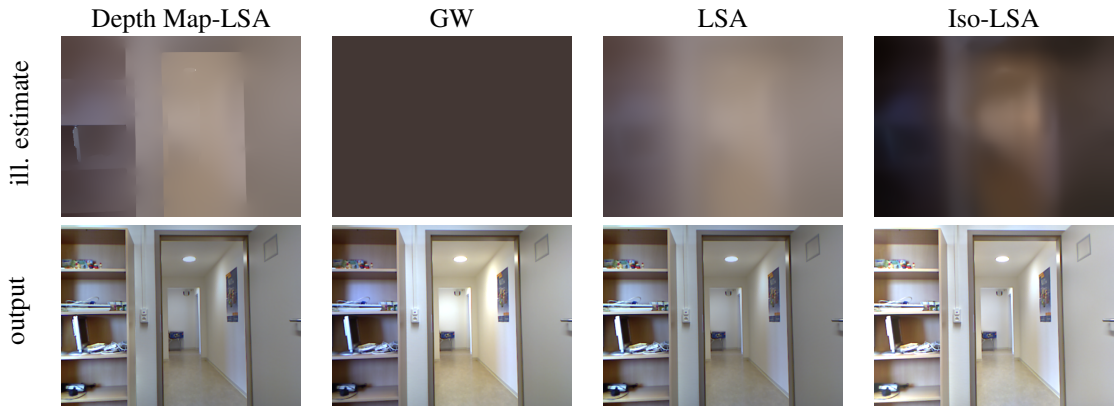

Figure 5: Comparison with three other color constancy algorithms for image 1: gray world assumption (GW), local space average color (LSA), computation of anisotropic local space average color along iso-illumination lines (Iso-LSA).

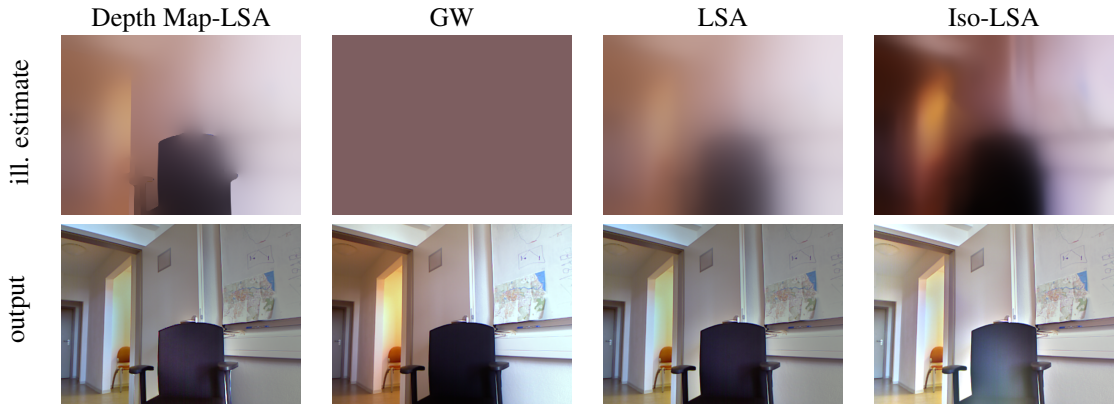

Figure 6: Comparison with three other color constancy algorithms for image 2: gray world assumption (GW), local space average color (LSA), computation of anisotropic local space average color along iso-illumination lines (Iso-LSA).

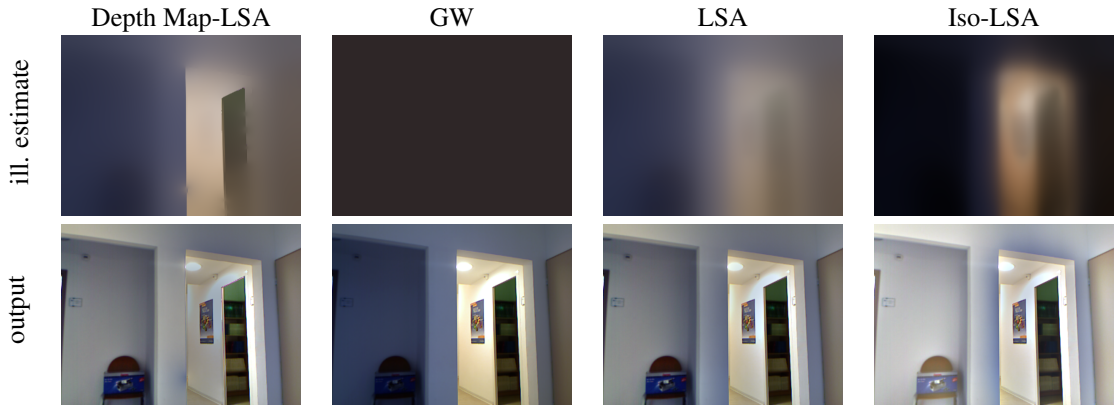

Figure 7: Comparison with three other color constancy algorithms for image 3: gray world assumption (GW), local space average color (LSA), computation of anisotropic local space average color along iso-illumination lines (Iso-LSA).

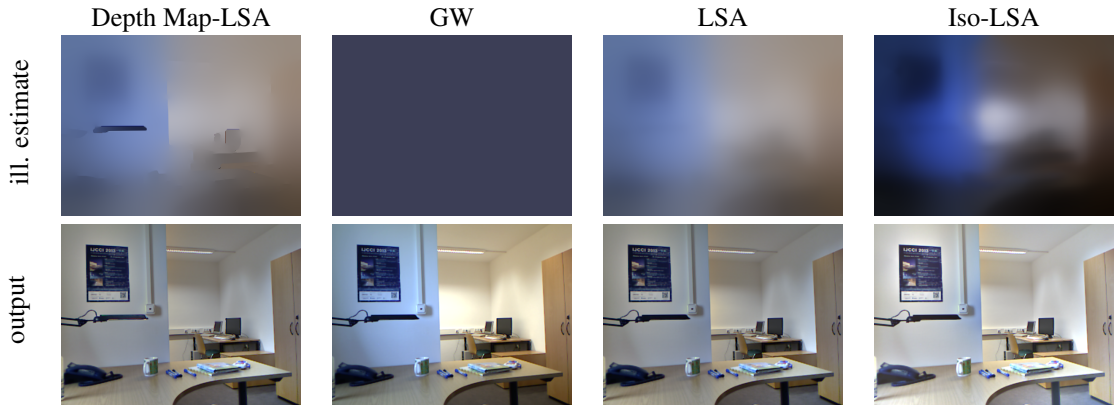

Figure 8: Comparison with three other color constancy algorithms for image 4: gray world assumption (GW), local space average color (LSA), computation of anisotropic local space average color along iso-illumination lines (Iso-LSA).